Extracting temporal relationships between weakly coupled peptidergic and motoneuronal signaling: application to *Drosophila* ecdysis behavior

Short title: Extracting relationships between weakly coupled neuronal signaling systems

Miguel Piñeiro[1‡], Wilson Mena[1,2‡], John Ewer*[1,3], Patricio Orio*[1,3]

[1] Centro Interdisciplinario de Neurociencia de Valparaíso, Universidad de Valparaíso, Valparaíso, Chile

[2] Department of Neuroscience, Institut Pasteur, 25 Rue du Dr Roux, 75015 Paris, France

[3] Instituto de Neurociencias, Facultad de Ciencias, Universidad de Valparaíso, Valparaíso, Chile

‡ These authors contributed equally

* Corresponding authors

E-mail: patricio.orio@uv.cl (PO), john.ewer@uv.cl (JE)

Abstract

Neuromodulators, such as neuropeptides, can regulate and reconfigure neural circuits to alter their output, affecting in this way animal physiology and behavior. The interplay between the activity of neuronal circuits, their modulation by neuropeptides, and the resulting behavior, is still poorly understood. Here, we present a quantitative framework to study the relationships between the temporal pattern of activity of peptidergic neurons and of motoneurons during *Drosophila* ecdysis behavior, a highly stereotyped motor sequence that is critical for insect growth. We analyzed, in the time and frequency domains, simultaneous intracellular calcium recordings of peptidergic CCAP (crustacean cardioactive peptide) neurons and motoneurons obtained from isolated central nervous systems throughout fictive ecdysis behavior induced *ex vivo* by Ecdysis triggering hormone. We found that the activity of both neuronal populations is tightly coupled in a cross-frequency manner, suggesting that CCAP neurons modulate the faster oscillation of motoneurons. To explore this idea further, we used a probabilistic logistic model to show that calcium dynamics in CCAP neurons can predict the oscillation of motoneurons, both in a simple model and in a conductance-base model capable of simulating many of the observed neural dynamics features. Finally, we developed an algorithm to quantify the motor behavior observed in videos of pupal ecdysis, and compared their features to the patterns of neuronal calcium activity recorded *ex vivo*. We found that the motor activity of the intact animal is more regular than the motoneuronal activity recorded from the *ex vivo* preparations during fictive ecdysis behavior; the analysis of movement patterns also allowed us to identify a new post-ecdysis phase.

Author Summary

Repetitive movements such as walking, swimming, and flying are controlled by networks of neurons known as central patter generators. In many cases, the exact pattern of activity is modulated by neuropeptides, which are small signaling molecules that, unlike neurotransmitters, are broadly released within regions of the nervous system. Because of this mode of action, it can be difficult to discern the relationship between the temporal pattern of firing of peptidergic neurons and the timing of the resulting motor behavior. Here, we developed methods to analyze the patterns of activity of such weakly coupled systems as applied to ecdysis, the stereotyped sequence of behaviors used by insects to shed the remains of their old exoskeleton at the end of every molt. Key actors in

this process are motoneurons (MN) and a set of neurons expressing the neuropeptide, Crustacean Cardioactive Peptide (CCAP). Combining real-time calcium imaging, frequency analysis, computational simulations, and image processing, we determined the relationships between the activity of CCAP neurons and the resulting motor output during pupal ecdysis in the fruit fly, *Drosophila melanogaster*. We found that several temporal features of the activity of CCAP neurons are highly coupled to the patter of activity motoneuronal pattern, suggesting an active role of CCAP neurons during ecdysis. We also developed quantitative approaches that allowed us to identify a new ecdysis sub-phase.

Introduction

Oscillatory neural circuits are important for many brain processes including memory formation [1,2], sensory representation [3–6], and rhythmic pattern generation [7,8]. Rhythmic movements are controlled by neuronal networks that time the firing of motoneuron discharges, which then cause a sequence of organized movements. In order to generate organized behaviors, it is necessary to coordinate dynamically the interaction of local and sparse brain circuits [9,10]. How these dynamic properties are tuned can profoundly influence the functional connectivity that defines the structure of neural circuits orchestrating behaviors. In this context, neuromodulators such as neuropeptides have been shown to play a major role in regulating and coordinating network functions in a number of processes including feeding, sleep, courtship, stress, learning and memory, amongst others [11–16].

Centrally coordinated innate behaviors have provided a useful model to study the molecules, neurons, and networks that organize sequential and rhythmic behaviors. One innate behavior that has been used for these studies is insect ecdysis, which is a stereotyped sequence of three motor programs (pre-ecdysis, ecdysis itself, and post-ecdysis) that is required to shed the remains of the old cuticle (exoskeleton) at the end of each molt [17–19]. Multiple neuropeptidergic circuits have been implicated in the regulation of the ecdysis but their precise roles are still poorly understood. Ecdysis begins with the release into the circulatory system (hemolymph) of the Ecdysis Triggering Hormone (ETH), which is synthesized and released from peripheral endocrine Inka cells [20]. Once ETH reaches the Central Nervous System (CNS) it sequentially activates several neuropeptidergics targets, where the network expressing the Crustacean Cardioactive Peptide (CCAP) has been suggested to be a critical

node for the generation of the ecdysial motor pattern [21–27]. However, the mechanisms by which the pattern of activity of the CCAP network is then translated into a motor output are not fully understood.

Recent advances in imaging technology enable the recording of neuronal activity in large regions of the brain including hundreds of neurons, thereby providing new ways to study circuit dynamics and behavior. Nevertheless, it remains challenging to extract quantitative information from such large data sets. It is thus necessary to develop suitable algorithms to determine the time windows in which specific motor activity occurs, and to identify the neurons that show activity related to the initiation and termination of a motor pattern. Previous approaches have used different methods to quantitatively classify neuronal activity patterns, which include principal components analysis (PCA), independent components analysis (ICA), singular-value decomposition (SVD), and k-means clustering, [28–30]. These methods have been widely used but they are often restricted to specific datasets. Therefore, the generation of more general methods would be of great utility to the field.

Here, we report on the implementation of new computational approaches to decode the signal dynamics driving ecdysis in the fruitfly, *Drosophila melanogaster*. We used mathematical methods and models to simultaneously analyze calcium imaging of CCAP neurons and motoneuron activity during the behavior. Although the pattern and the timing of activity of these two populations of neurons differed significantly, we were able to show that the activity of CCAP neurons is functionally tightly coupled to that of the motoneurons during the ecdysis and post-ecdysis phases, in a cross-frequency manner. This allowed us to fit a probabilistic logistic model to the experimental data in order to predict the times when motoneurons had a high chance of oscillating. We also generated a conductance-based model that simulates many of the experimentally features observed. Finally, we developed an algorithm that extracts the major traits of ecdysis behaviors, allowing us to quantify the movements that occur during the behavior of the intact animal and contrast them with the *ex vivo* recorded motoneural activity. This algorithm also allowed us to identify a new sub-phase within the post-ecdysis period. In summary, we describe a series of methods to quantify and correlate patterns of neuronal activity with differing temporal characteristics that occur during the expression of a stereotyped behavior. Using these methods, we show that the CCAP network tightly regulates motoneuronal activity through the execution of the entire ecdysis and post-ecdysis routines.

RESULTS

INDIVIDUAL DYNAMICS OF CCAP-EXPRESSING NEURONS AND MOTONEURONS

The pattern of neural activity that corresponds to ecdysis behavior can be elicited in *ex vivo* preparations of *D. melanogaster* CNS by exposure to ETH. We followed this approach using CNSs from animals just prior to pupal ecdysis, which expressed the genetically-encoded calcium sensor GCaMP3.2 (as a proxy for neural activity), either in CCAP neurons or in both CCAP neurons and motoneurons (Fig 1a, b, c). As has previously been reported [22,25], increases in GCaMP signal typically began 20 minutes after stimulation with ETH, around the time of ecdysis phase is induced in intact pupae. During this phase, CCAP neurons and motoneurons display higher levels of activity, which then falls after entering the post-ecdysis phase.

Fig 1: CCAP neuron and motoneuron activity

(a) Single-plane calcium imaging of GCaMP3.2-expressing CCAP neurons. **(b)** Projection of 5 images from different planes, of GCaMP3.2-expressing CCAP neurons and motoneurons. **(c)** Time series of signal from calcium sensor of AN1-AN4 α CCAP neurons and motoneurons recorded from a single CNS; time zero corresponds to moment of ETH-stimulation. The letter indicates the side (left [L] and right [R]), while the number indicates the abdominal segment of the neurons. **(d)** Mean time of onset of α CCAP neuron and motoneuron activity, for each of 9 separate experiments, showing temporally close values between populations. “MN” and “CCAP” indicate motoneurons and α CCAP neurons, respectively. **: p-value < 0.01, ***: p-value < 0.001.

CCAP neurons can be divided into α and β neurons depending on their location and their activity pattern [25]. Here, we mostly focused on the α type, because β neurons appeared to display a low pass-filtered version of the α activity. Regarding motoneurons, we divided them into left and right regions, as there were no major differences in the activity between sides. Grouping them also increased the signal-to-noise ratio (SNR), making the task of comparing different experiments easier.

In the intact animal, the onset of left-right alternating motoneuronal activity corresponds to the beginning of the ecdysial phase proper of the ecdysis motor sequence [22,25]. As a first approach to characterize the dynamics of CCAP neuron and motoneuron activity, we computed the onset of their activity in preparations in which both

122 classes of neurons expressed the GCaMP3.2 calcium sensor. The mean onset time after ETH challenge was
123 1176 ± 37.9 s for the α CCAP neurons and 1149 ± 61.5 s for the motoneurons (Fig 1d) (n = 9).

124 The mean onset of activity in α CCAP neurons and motoneurons tended to be temporally correlated. Indeed, for
125 all experiments except one, the onset of activity in α CCAP neurons and in motoneurons was significantly close in
126 time (p-values < 0.01; one-tailed Mann-Whitney U test). In contrast, when comparing the onset time of α CCAP
127 and motoneurons from different experiments, we found that they were more temporally separated. In addition, the
128 onset of motoneuron activity usually lagged behind that for CCAP neurons, suggesting that some level of α CCAP
129 activity is required to initiate the motoneuronal oscillatory activity.

130 Next, we computed the period of the oscillations of both populations of neurons using the continuous wavelet
131 transform (CWT). This method was preferred over the Fourier transform, as CWT can localize the frequency
132 components in time. The average scaleograms of all α CCAP neurons (n = 111) (Fig 2a) and motoneuron time
133 series (n = 18) (Fig 2b) showed that the main oscillatory period was around 50 to 200 s for α CCAP neurons, and
134 around 25 to 50 s for motoneurons.

135

136 **Fig 2: Oscillation period of CCAP neurons and motoneurons**
137 **(a, b)** Average scaleogram for all α CCAP neuron (**a**) and motoneuron time series (**b**). **(c)** Mean oscillation
138 periods of CCAP neurons and motoneurons for all 9 experiments. For CCAPs, only the data for neurons that
139 passed the selection criteria are shown (see text). In some experiments none were accepted, and the bar is
140 missing. By contrast, in all experiments motoneurons of the left and right regions showed a dominant oscillation
141 period.

142

143 Nevertheless, not all α CCAP neurons showed a clear single dominant frequency component. Applying a criterion
144 for the existence of predominant peaks in the frequency spectrum (minimum amplitude at each side of the interval
145 that goes from half to twice the period of the maximum amplitude, to be less than 80% of the maximum) we found
146 that only 47% of the α CCAP neurons passed the selection criterion, illustrating the irregularity of the oscillatory
147 activity in these neurons. Neurons that passed this criterion were used to compute the mean period of each

148 experiment (166 ± 23.3 s; n = 13 experiments); the remaining neurons were eliminated from further frequency
149 analysis.

150 By contrast to CCAP neurons, motoneurons displayed a more regular pattern of activity with a clearer main
151 oscillatory component, and no motoneuron time-series was discarded. The main oscillatory period of
152 motoneurons was 33.4 ± 4.1 s (n = 9). The difference in the principal oscillatory period between the left and right
153 sides was also small, suggesting that the activity of motoneurons on both sides is not independent. We plotted the
154 periods of both CCAP and motoneurons and their means (Fig 2c), and in all experiments found that the period of
155 motoneuron activity was much shorter than that of CCAP neurons.

156

157 ## COORDINATION WITHIN CCAP EXPRESSING NEURONS

158 To investigate the coordination between CCAP neurons, we measured the linear relationship between their time
159 series using Pearson's correlation. We grouped the correlation pairs into functionally equivalent pairs based on
160 what is known about their anatomy, as well as their synaptic and peptidergic connectivity [31,32]. Thus, the
161 correlation pairs were grouped into: contralateral neurons (on the same segment but opposite sides), ipsilateral
162 neurons (on the same side but in different segments), and “other” neuron pairs (on opposite sides and on a
163 different segments) (see Fig 3a). We computed the group p-values using the one-tailed Mann-Whitney U test to
164 compare correlations of each experiment to null cross-experiment correlations. In all cases we obtained p-values
165 < 0.001 making group correlations shown in Fig 3b-f highly significant.

166

167 **Fig 3: CCAP neuron coordination**

168 **(a)** Pearson’s correlations pairs are divided into 3 groups: contralateral neurons (“C”), ipsilateral neurons (“I”), and
169 “others” (“O”). As an example, the graph shows pairs that include the left AN2 neuron. **(b-j)** Correlation
170 coefficients between the time series of CCAP neurons, shown as violin plots with their minimum, maximum and
171 mean values. **(b)** α CCAP neuron correlations in the time domain. **(c)** β CCAP neuron correlations in the time
172 domain. **(d)** α-β CCAP neuron correlations in the time domain. **(e)** Correlations of α CCAP neuron amplitude of
173 oscillations in the time-frequency domain. **(f)** Correlation of α CCAP neuron amplitude and phase in the time-

174 frequency domain. **(g-j)** Correlation between ipsilateral pairs with different segmental separation, “I1”, “I2” and
175 “I3” groups are contiguous, separated by 1 and separated by 2 segments, respectively. The plots use the same
176 notation as the plots in **(b-f)**. *: p-value < 0.05, **: p-value < 0.01, ***: p-value < 0.001.

177

178 Correlations between contralateral CCAP neurons were higher than between ipsilateral neurons, for αα and αβ
179 pairs (Fig 3b,c,d). The correlations between contralateral neurons were also higher than between “other” neurons
180 for αα, ββ and αβ pairs. To test if the distance (in segments) between neurons affected the strength of the
181 coupling, we divided the pairs into 3 ipsilateral groups based on their segment separation. The I1, I2 and I3
182 groups contain ipsilateral pairs of neurons within the same segment, or pairs separated by 1 or by 2 segments,
183 respectively. We performed the same analyses on these groups (Fig 3g-j), and found that correlation for both αα
184 and αβ neuron pairs dropped as the segmental distance between them increased (Fig 3i,j). In contrast,
185 coordination between ββ neuron pairs was not affected by segmental distance (Fig 3h).

186 Finally, we studied the correlation of the αα pairs in the time-frequency domain, using the 50 to 200 s period band
187 of the CWT. This also allowed us to study the correlation of the oscillation’s amplitude with and without the phase
188 component. We found that contralateral neurons had a higher correlation of amplitudes (absolute value of the
189 CWT) compared to the other pairs (Fig 3e). When taking into account the phase component (the real part of the
190 CWT) the correlation coefficients displayed an important drop, showing that the phase of the oscillations was
191 poorly coordinated (Fig 3f). The interpretation of these results is that CCAP neurons tend to be active at the same
192 time but do not oscillate with the same phase.

193 These results show that all abdominal segments 1-4 (AN1-AN4) CCAP neurons tend to have synchronized
194 activity, but that their coupling strength varies depending on the neuronal pair considered. Contralateral αα and αβ
195 pairs from the same segment appear to show higher coupling, whereas ββ pairs show similar contralateral and
196 ipsilateral coupling strength. Finally, the correlated activity does not involve a synchronized oscillation, i.e. CCAP
197 neurons oscillate at the same time but not in a concerted fashion.

198

COORDINATION BETWEEN MOTONEURONS

Left and right motoneuronal regions express coordinated but opposite activity. In order to quantify this coordination and determine how it evolves over time, we calculated the Pearson's correlation between left and right motoneuron regions on a sliding window of 100 s (thus the window is longer than the oscillation period, but shorter than the duration of oscillation bursts). The correlations tended to be negative during the oscillating periods and positive during the non-oscillating periods (Fig 4a), consistent with the observed synchronous but phase-opposite behavior.

Fig 4: Motoneuronal coordination

(a) Correlation coefficients between left and right motoneuron time series, calculated over a sliding window of 100 s. Time series for left ("MN L") and right ("MN R") motoneuronal regions are shown in orange and purple, respectively, and the Pearson's correlation coefficient ("r") of the sliding window is shown in black. Gray horizontal lines indicate correlations of −1, 0 and +1. **(b)** Example of the method used to compute the mean phase difference of an experimental recording. Blue and green points represent the phase difference at every instant of the experiment; their amplitude is scaled to the mean amplitude of the oscillations of the left and right region. The red point represents the mean vector, whose phase represents the mean phase difference of the experiment. **(c)** Mean phase difference for 9 experiments (blue) and mean for all experiments (red).

We then used the CWT to compute the instantaneous amplitude and phase of the motoneurons' primary oscillatory period for the entire recording. We generated vectors with angles equal to the phase difference and lengths equal to the mean amplitude of their CWT, computing the phase difference of the regions by averaging all the vectors of the experiment (Fig 4b).

Using this procedure, we found a large amount of variability in the phase difference within each experiment, and an important spread of the experimental mean phase difference (Fig 4c), with a global mean of 182.1 ± 14.6°.

The fact that the motoneurons oscillate in antiphase is compatible with the existence of a central pattern generator (CPG) downstream of the CCAP neurons [27]. The variability in the phase difference could be an

indicator that the CPG imaged in the calcium imaging preparations has difficulty synchronizing left and right motoneurons in the absence of sensory feedback, analogous to what has been shown previously for *Drosophila* larval crawling behavior [33].

FUNCTIONAL CONNECTIVITY BETWEEN CCAP NEURONS AND MOTONEURONS

We noticed that α CCAP neurons appear to modulate the amplitude of the motoneuronal activity, with high levels of α CCAP neuron fluorescence tending to match periods of motoneuronal oscillation. Based on this observation, we converted the motoneuronal signal so that it could be correlated quantitatively to that of CCAP neurons. For this we used a single motoneuronal signal made by subtracting the time series of one region from the other. This procedure reduced the common noise and increased the SNR and oscillation amplitude, without much loss of information as the two-time series are mostly redundant.

We computed the absolute value of the CWT of the motoneuronal signal at its previously computed primary oscillatory period, thus extracting the instantaneous amplitude (**Error! Reference source not found.**a). The amplitude signal from the motoneuronal oscillation was then correlated using Pearson's correlation to each α CCAP neuron time series. The significance of the within-experiment correlations, as compared to null cross-experiment correlations, was tested using a one-tailed Mann-Whitney U test. For all experiments except one, the correlations were significant (Fig 5b). The single experiment that did not display significant correlations showed post-ecdysis motoneuronal oscillations that did not match temporally the increases in α CCAP neuron activity.

Fig 5: Correlation between α CCAP neuron and motoneuron activity

(a) Orange and purple lines show the activity of the left ("MN L") and right ("MN R") motoneuron regions, respectively, and the black line ("Activity") shows the amplitude of the motoneuron signal. **(b)** Correlation coefficients between α CCAP neurons and the amplitude of the motoneuronal time series, shown as points and the means as bars. **(c)** Analogous to **(b)**, but with the pre-ecdysis phase removed. *: p-value < 0.05, **: p-value < 0.01, ***: p-value < 0.001.

As the time of onset of activity varied across experiments, it could be argued that the high significance of the correlation between α CCAP neurons and motoneurons is caused by the matching of onset times. To test this hypothesis, we removed the initial non-oscillatory block for each experiment and repeated the analysis using the modified time series (**Error! Reference source not found.**c). For all experiments except two, the results were significant, suggesting that α CCAP neurons regulate the motoneuronal activity during the entire recording period.

These results suggest that the CPG responsible for ecdysis requires a constant input from the α CCAP neurons to maintain its ongoing oscillatory activity, consistent with previous findings [21,27]. Also, the correlated activity allows us to talk of *functional connectivity* [34] that occurs between CCAP and motoneurons, regardless of whether there is a structural connectivity (synapses) between them.

FITTING THE CCAP-MOTONEURON INTERACTION WITH A LOGISTIC MODEL

After finding that CCAP neurons are functionally coupled to the motoneurons, we built a model to test how well the activity of the α CCAP neurons could predict the motoneuronal oscillatory state.

The model takes the activity of α CCAP neurons as input and generates the motoneuronal oscillatory activity as output. As the amplitude of the motoneuron oscillations does not appear to be regulated by α CCAP neurons, we employed a binary signal obtained by thresholding the oscillation amplitude (see Methods) to describe the oscillatory and non-oscillatory motoneuronal activity. The motoneuron oscillation generator (CPG) integrates the signals from AN1-AN4 α CCAP neurons and produces a probabilistic oscillatory response.

The system was modeled as a logistic regression:

$$p(t) = \frac{1}{1 + \exp(-\beta - \sum_{i=1}^{8} w_i f_i(t))}$$

Where $p(t)$ represents the probability that motoneurons will oscillate at time t; $\mathrm{f_i(t)}$ the i-th α CCAP neuron time series; $\mathrm{w_i}$, the weight of the i-th α CCAP neuron; and β the offset. The model's coefficients were estimated using maximum likelihood estimation (MLE) with the constraint that all weights must be positive.

As shown in **Error! Reference source not found.**a,b, the maximum likelihood solution has weights set to zero, i.e., not all the CCAP neuron time series of every experiment are needed to predict the motoneuronal oscillations. The minimum number of α CCAP neurons required to reach the maximum likelihood was 2, the maximum was 6 and the average was around 4. These results should not be interpreted to mean that some α CCAP neurons do not have any effect on the motoneuronal oscillatory activity; rather, we expect the redundancy of their activity to make the likelihood of the model to be maximized with only some of them. The weights were highly variable, also an indicator of the degeneracy in the system, as α CCAP neurons with diverse activity dynamics nonetheless generate similar motoneuronal activity.

Fig 6: Fit of the logistic model to the experimental data

(a, b) Time series of α CCAP neurons (red, blue), motoneurons (orange, purple), binarized oscillatory activity of motoneurons (black), and probability of oscillation predicted by the model (green). CCAP activity traces are shown in red with their corresponding weight value if it is positive ("CCAP (Wi > 0)"), or in blue with no value if it is zero ("CCAP (Wi = 0)"). All weight values were computed through multi-weight model fitting. **(a)** Example of a good match between the model p(t) and the oscillatory state of the motoneurons. **(b)** Example of a poor match during the post-ecdysis phase, as a result of the lack of α CCAP activity.

Error! Reference source not found.a shows that during the oscillatory activity of motoneurons, $p(t)$ increased accordingly; one exception can be observed in **Error! Reference source not found.**b, where the $p(t)$ barely increased during rare post-ecdysis oscillatory events, due to the lack of significant increases in the activity of the α CCAP neurons during this period events (this is the same experiment that showed poor correlation between CCAP and motoneuron activity).

We also fitted a single weight model (same value for all w_i), based on the assumption that all α CCAP neurons affected motoneuronal activity in the same way. To select the best model by taking into account the tradeoff between the goodness of fit and the complexity of the model we used the Akaike Information Criterion (AIC) [35]. For all 9 experiments the multi-weight model performed noticeably better (i.e., its values were lower) than did the

single-weight model. This suggests that not all CCAP neurons have the same impact on the motoneuronal time series; the origin of this could be experimental, biological, or a combination of the two.

	Experiments								
	1	2	3	4	5	6	7	8	9
Single-weight	908	1803	1092	1519	3714	2976	2312	1489	3108
Multi-weight	711	1598	888	891	2481	2464	2019	1227	2675

Table 1. Akaike information criterion. AIC values of single- and multi-weight model fittings of every experiment.

REPRODUCING MOTONEURON CALCIUM ACTIVITY USING A CONDUCTANCE-BASED MODEL

A logistic model is an abstract model that can fit a probability function to a binary motoneuron oscillation time series; however, it is not capable of modeling calcium dynamics. To test if we could reproduce the observed calcium dynamics, we used a model developed by Jalil et al., 2010, consisting of two endogenously bursting neurons with fast non-delayed inhibitory connections that synchronize in antiphase. The activity of the neurons depends on the voltage-dependent potassium and sodium currents and on reciprocally inhibitory synapses between them. To couple the oscillatory activity of the model to the CCAP neurons, we added a depolarizing current that depends on the activity of the α CCAP neurons. The model was further adapted to generate fluorescence spikes during the phase of motoneuronal oscillation, matching the oscillation timing, the calcium interspike interval (ISI), the spike phase difference, and the time constant of each experiment (see methods).

In our model, 8 α CCAP neurons are coupled to 2 motoneurons (**Error! Reference source not found.**a) and each α CCAP neuron releases a peptidergic signal that depolarizes the motoneurons and causes them to oscillate. α CCAP neurons release the signal according to the recorded fluorescence time series factored by a

weight (already computed in the logistic model). Outputs from the peptidergic neurons are then multiplied by weights, summed, and transformed with a logistic function to generate the gating variable $p(t)$. In this way, α CCAP neurons modulate the oscillatory behavior of the motoneurons through $p(t)$.

Fig 7: Simulation of fluorescence spikes.

(a) Model circuit structure, showing the 8 α CCAP neurons that release the peptidergic signal (black circles) and activate the oscillatory behavior of the reciprocally inhibiting motoneurons. **(b)** Simulated fluorescence (top) and voltage (bottom) time series of left ("Sim L") and right ("Sim R") motoneurons. **(c)** Magnification of a small temporal segment of (b). **(d, e)** Simulation of two different experiments. The gray grid marks probabilities of 0, 0.5 and 1. "MN L", "MN R", "Sim L" and "Sim R" indicate experimental left, experimental right, simulated left, and simulated right motoneurons, respectively. $p(t)$ indicates the probability of oscillation.

We fitted the model during multiple passes of manual parameter adjustments and simulation sessions. The resulting parameter values were identical for all experiments except for τ_f and τ_K, which were used to fit the exponential decay and oscillation period, respectively.

An example of the bursting behavior of the model is shown **Error! Reference source not found.**b, where motoneuron fluorescence and voltage are plotted next to each other for comparison and shows that the simulated fluorescence increases during the bursting phase and decreases during the non-bursting phase. When the model is run using experimental CCAP time series as its inputs, it can reproduce fairly well the motoneuron oscillatory behavior (Fig 7d,e). The timing of the simulation oscillations approximately matches that of the experiments, even during the periods of lower spiking frequency. This is especially interesting considering that $p(t)$ was fitted to a binarized (as opposed to a graded) motoneuronal activity signal. Another noteworthy result is that, as more time passes after an oscillation, the neurons are more likely to begin oscillating again. This effect is the result of the slow dynamics of the potassium current, which slowly stops inhibiting action potentials (APs); this can be seen in the last oscillation period in Fig 7d.

The simulation spike frequency and its exponential decay matched that of the experiments, as they were fitted through the τ_{Na} and τ_f parameters. The noise caused by equation (7) adds amplitude and phase variability, resembling the one observed in the experiments.

Fig 8 compares simulated and experimental motoneuron time series for 3 different experiments in the time and time-frequency domains. To reduce the noise of the model scaleogram, each simulation was repeated 10 times and their scaleograms averaged. In all experiments the simulations showed a good time-frequency match to the experimental data.

Fig 8: Simulations of the Logistic model linked to a conductance-based bursting model

(a) Experimental and a simulation time series of 3 experiments. “MN L”, “MN R”, “Sim L” and “Sim R” indicate the left and right experimental, and left and right simulated motoneuron activity respectively. **(b)** Corresponding scaleograms, except that the scaleogram simulations are the average of 10 simulations. Each row shows the experimental (bottom) and the simulated (top) motoneuron activity, respectively.

Even though very little is known about the structure of the circuit, our model replicated many of the features of the activity pattern observed in the experimental recordings, showing that the activity of CCAP neurons is tightly linked to that of motoneurons.

CORRESPONDENCE BETWEEN CALCIUM ACTIVITY AND MOTOR BEHAVIOR

Finally, we wanted to quantify how much the neural activity of the *ex vivo* CNS during fictive ecdysis accurately reflected the *in vivo* ecdysis motor behavior. To do this, we analyzed the pupal ecdysis motor behavior of intact animals removed from their puparium. The analytic process is divided into three phases: computation of the position of midline of the pupa, generation of the time-space diagram, and quantification.

To compute the midline of the pupa, a sequence of image processing operations was applied to every frame of the video. (See Fig 9Fig 9 and further details in Methods). The result is a time series indicating the position of the midline of the pupa with respect to the lateral axis, at each position along the antero-posterior axis.

370

371 **Fig 9: Midline computation**

372 Sequence of image processing steps used to compute the midline of the pupa for every frame of the video. An
373 RGB video frame is extracted **(a)** and converted to a grayscale image **(b)**, then thresholded **(c)** and its holes filled
374 **(d)**. Blob borders are softened by applying a gaussian filter **(e)** and thresholded again **(f)**. Small blobs are
375 discarded **(g)** and the left (green) and right (red) borders are computed **(h)**. The mean of the two borders
376 represents the midline (white line).

377

378 The varying position of the midline was used to generate a time-space diagram, where time is mapped in the
379 horizontal axis and the antero-posterior axis is mapped along the vertical axis. The color code indicates the
380 position of the midline along the lateral axis. The diagram shows a distinctive pattern for each major motor pattern
381 (Fig 10a). Peristaltic motor activity begins in the anterior and propagates to the posterior region of the animal,
382 generating descending line patterns (from top-left to bottom right). The swinging motor pattern is characterized by
383 a large variation of the midline position in the anteroposterior mid-section and a lengthening and shortening of the
384 diagram across the anteroposterior axis. The lengthening occurs when the pupa is straight and the shortening
385 when it bends to the side. Finally, the stretch-compression activity generates variation of the diagram across the
386 anteroposterior axis like the swinging pattern, but with minimal variation of the midline position in the mid-section.

387

388 **Fig 10: Behavioral analysis**

389 **(a)** Time-space diagram patterns generated by three different motor routines. The “AP axis” represents the
390 anteroposterior axis, which is oriented so that the top of the diagram corresponds to the anterior side of the pupa.
391 The color indicates the position of the midline in the left-right axis along the anteroposterior axis, with the top and
392 bottom of the diagrams corresponding to the anterior and posterior sections of the midline, respectively. Darker
393 colors indicate that the midline section is closer to the left side, whereas lighter colors indicate that it is closer to
394 the right side. **(b)** Filtered time-space diagrams of 6 pupal recordings aligned to the time when the ecdysis phase
395 began. White spaces in the top diagram correspond to times when the pupa moved outside the microscope
396 viewing field. **(c)** Time series of the mid-section of **(b)** (“LR axis” represent the left-right axis).

We processed using this procedure 6 videos of pupal ecdysis behavior and generated the corresponding time-space diagrams (Fig 10b) and time series of the mid-sections (Fig 10c). Since pupae were not stimulated with exogenous ETH at the beginning of the video (as was the case for calcium recordings), we aligned the diagrams and time series to the beginning of the ecdysis phase.

All 6 time-space diagrams showed a similar pattern with very small differences in their timing and period. Quantifications were done manually by measuring time in the time-space diagram and time series plots (**Error! Reference source not found.**). To measure the period, we measured the duration of the largest time span of full cycles and divided it by the number of cycles. A swinging cycle was defined as a bending to one side followed by a bending to the opposite side. During post-ecdysis, a cycle included the bending to both sides followed by the stretch-compression motor pattern.

Fig 11: Behavioral metrics

Metrics and comparison of the motoneuronal activity (n = 9) and pupal behavior (n = 6). **(a)** Period of the characteristic motor patterns of each of the ecdysial phases. **(b)** Duration of the ecdysis and of the fast post-ecdysis phase.

Finally, we compared the metrics obtained from the behavior of the intact pupal preparations to those of the motoneuron activity in the *ex vivo* CNS preparations (**Error! Reference source not found.**). The pre-ecdysis peristaltic contractions period of the pupa averaged 59.4 ± 8.7 s. We were able to visually detect the motoneuron peristaltic activity in the motoneuronal recordings, but because of the low SNR and time resolution, its quantification was not reliable.

The ecdysis swinging contraction period was significantly shorter in the motoneuronal recordings than in the pupal recordings (25.1 ± 2.4 s versus 45.7 ± 3.2 s, respectively; p-value < 0.002, two-tailed Mann-Whitney U test). The mean duration of the ecdysis phase, on the other hand, was not significantly different (346.7 ± 37.8 s versus 363.2 ± 31.2 s, respectively).

The mean post-ecdysis cycle period was 128.8 ± 37 s in the motoneuronal recordings. In intact animals, in contrast, we noticed that the post-ecdysis phase could be divided into two subphases: a fast one followed by a slow one. Both subphases included alternations between periods of swinging and periods of stretch-compression contractions, but in the slower phase the stretch-compressions tended to be of longer duration. The mean period was 76.4 ± 2.4 s for the fast and 187.3 ± 9.6 s for the slow subphases, respectively. We compared the mean of the three groups and found significant differences only between the slow and fast post-ecdysial phases (p-value < 0.004, two-tailed Mann-Whitney U test). The mean duration of the fast post-ecdysis phase was 724.1 ± 22.1 s. The slow post-ecdysis phase duration could not be measured as it persisted past the end of the recording time.

In summary, we found that most of the activity recorded during pupal ecdysis behavior in intact animals had a fictive counterpart, but the *ex vivo* motoneuronal recordings showed different timing and greater irregularity. This indicates that the neural circuit controlling ecdysis behaves differently when tested in isolation, suggesting that sensory feedback could play an important role in regulating the timing of the ecdysis sequence.

Discussion

Ecdysis behavior consists of 3 separate motor programs (pre-ecdysis, ecdysis and post-ecdysis) that are expressed in a specific temporal order. A successful ecdysis is the result of the interplay between peptidergic neurons and motoneurons, each with quite different temporal patterns of activation. Here, we have combined calcium imaging recordings, computational tools, and behavioral analyses to gain better insights into the functional relationships between these two neuronal populations.

Our results suggest that CCAP neurons trigger motoneuronal activity and also sustain it throughout the ecdysis and post-ecdysis subroutines. Moreover, our analyses reveal a cross-frequency interaction between these two neuronal populations, as the slow variations in CCAP activity is correlated with the faster oscillations of motoneurons. This raises the question: What is the advantage of having CCAP neurons continuously modulating motoneuronal outputs? One possible answer is that it provides a continuous control over the desired behavior, allowing feedback mechanisms or environmental conditions to modify it. Our analyses show that the activity patterns of CCAP neurons correlate with different motor outputs: high CCAP activity generates swinging contractions over the ecdysis phase, whereas the alternation between high and low amplitude CCAP responses

449 signals the transition from swinging contractions to stretch-compression movement, which are distinctive of post-
450 ecdysis. Thus, specific CCAP activity patterns could be triggering the release of neuropeptides and potentially
451 neurotransmitters in an activity-dependent way to modulate diverse motor outputs. It has been reported that co-
452 transmitters have distinct activity thresholds for their release, providing opportunities for circuit flexibility. For
453 example, a low, tonic firing frequency may result in the release of neurotransmitters, whereas rhythmic bursting
454 pattern may cause the release of both neurotransmitters and neuropeptides [37]. Consequently, a firing rate-
455 dependent response would generate the modulation of diverse post-synaptic outputs [38–40]. To confirm that the
456 CCAP activity pattern is modulating the release of neuropeptides or neurotransmitters in an activity-dependent
457 way throughout ecdysis, an *in vivo* characterization of neuropeptide-neurotransmitter release associated to
458 specific activity patterns and behavioral phases would have to be undertaken.

459 We showed that the activity of CCAP neurons can be aligned with motoneuron oscillatory activity using both an
460 abstract logistic model and a conductance-based model. Using these models, CCAP activity could accurately
461 predict motoneuronal oscillatory activity (error rate <10%). In addition, the models showed that in general only 4
462 CCAP neurons or fewer (of a total of 8), were required to predict the start of an oscillatory episode. A possible
463 explanation for this result is related to redundancy within the CCAP ensemble. In *Drosophila*, the CCAP AN1-AN4
464 network consists of 16 neurons that have been largely characterized from a molecular to a functional point of view
465 [22,23,25,27]. The functional redundancy predicted by our model can have two interpretations. On one hand, it is
466 possible that only one half of the CCAP AN1-AN4 cells may be necessary and sufficient to trigger ecdysis and
467 post-ecdysis phases, with the rest of the network adding robustness and flexibility to the control of motoneuronal
468 oscillations. Alternatively, all CCAP AN1-AN4 neurons may be necessary for the oscillatory command to reach the
469 entire motoneuronal population. In this case, the statistical redundancy emerges just because of their coordination
470 and synchronization. These two scenarios could be distinguished experimentally, through the selective
471 inactivation of one or more CCAP neurons using recently developed holographic optogenetic tools [41–43].

472 With the addition of a simple conductance-based bursting CPG model [36,44], we were able to replicate the
473 motoneuronal oscillatory activity. In the absence of any electrophysiological information about the neurons that
474 generate this rhythm and the ion channels involved, we chose a simple generic neuronal oscillator. However, the
475 well-known degeneracy and diversity found in oscillation-generating circuits [45–47] implies that many different

476 neuronal models could produce the same output. It also implies that it is virtually impossible to make a better
477 prediction without further electrophysiological evidence, and moreover, that the details of mechanisms found in
478 different species can diverge significantly. Our analysis methods provide a framework to interpret new
479 experimental manipulations that can be made to the mechanisms downstream the CCAP command signal.

480 The 3 different motor programs of ecdysis can be observed in puparium-free preparations. Until now, these
481 components have been qualitatively characterized only on the bases of obvious motor changes [22,25]. Our
482 computational method allowed us to quantitatively characterize the ecdysis and post-ecdysis behavioral programs
483 and to contrast them with the associated motoneuronal activity. These analyses showed that most of the activity
484 observed during pupal behavior had its fictive counterpart in the *ex-vivo* preparation. However, the patterns of
485 motoneuronal activity were more variable compared to the behavior observed in the intact animal. This mismatch
486 could be caused by sensory feedback, which has been shown to be critical for the proper organization of motor
487 programs in many animals [33,48,49]. Sensory information may impact CCAP network activity itself or,
488 alternatively, that of downstream CCAP targets. One possible source for this sensory (proprioceptive) feedback
489 are somatosensory neurons located along the body wall of the pupa. In this regard, computational modeling of the
490 neural circuits involved in the production of peristaltic waves during larvae crawling, have showed that adding
491 sensory feedback to a CPG network model affects both speed and intersegmental phase relationships [50].
492 Moreover, recent experimental work supports the idea that proprioceptive feedback plays a key role on the proper
493 coordination of muscle contraction and on the speed of wave propagation [51]. Additional work must be done in
494 order to identify the potential proprioceptive pathway that modulates the ecdysis motor sequence.

495 Finally, our algorithm also detected that post-ecdysis phase can be divided into fast and slow contraction
496 frequencies. This newly detected motor program seems to be absent from our Ca^{+2} imaging recordings,
497 suggesting that additional network layers between CCAP and motoneurons may potentially be involved, whose
498 activity pattern has not yet been detected or characterized. Using our computational tools, future experimental
499 research will be able to quantitatively relate this second post-ecdysis phase to the activity of other neural
500 populations or gene expression networks.

501

METHODS

Fly lines

Drosophila melanogaster cultures were raised on standard agar/cornmeal/yeast media and housed at 22-25°C. The following GAL4 drivers were used: *Ccap*-GAL4 (driver for CCAP neurons; [52]) and C164-GAL4 (driver for motoneurons; [53]). We obtained the genetically encoded calcium sensitive, GCaMP3.2, from Julie Simpson (Janelia Farm, USA). GCaMP3.2 was expressed in CCAP neurons and motoneurons simultaneously by combining the *Ccap*-GAL4 and C164-GAL4 drivers using standard techniques.

Imaging of calcium dynamics

Calcium (Ca^{2+}) recordings were carried out essentially as described in Mena *et al.* [25]. Briefly, animals containing a bubble in the mid-region of the puparium (~4 hours before pupal ecdysis) were selected. The central nervous system (CNS) was dissected in cold PBS, immobilized in 1.5% low melting temperature agarose solution (Sigma type VII-A; Sigma-Aldrich Chemical Co., MO) and covered with Schneider's Insect Medium (Sigma-Aldrich Chemical Co., MO). Recordings were performed using an Olympus DSU Spinning Disc microscope (Olympus Corporation, Shinjuku-ku, Tokyo, Japan) under a 20 X W NA 0.50 immersion lens. GFP signal was acquired using an ORCA IR2 Hamamatsu camera (Hamamatsu Photonics, Higashi-ku, Hamamatsu City, Japan) using the CellR Olympus Imaging Software (Olympus Soft Imaging Solutions, Munich, Germany). Fictive ecdysis was triggered by adding 600 nM of ETH1 (Bachem Co., USA). We recorded multiplane fluorescence using a sampling rate of 1 picture every 2-3 second for at least 60 min. Depending on the preparation, the number of images per z-stack was 3-5 focal planes (covering 100-200 μm in depth), which allowed the entire motoneuronal and CCAP network to be imaged.

Video pre-processing

Video sequences were first processed using ImageJ [54]. Calcium time series were first detrended in order to compensate for slow variations of fluorescence during the recording caused by tissue drifting, then normalized in order to make the time series more uniform in terms of the minima and maxima of fluorescence. Detrending was performed by finding the minimum values during the first and the last 250 s of the time series, generating a line that crossed those points, and subtracting the corresponding value from each frame. The normalization linearly mapped the time series so that the minimum and maximum values were 0 and 1, respectively.

$$m = \frac{f(t_1) - f(t_0)}{t_1 - t_0}$$

$$g(t) = f(t) - mt$$

$$h(t) = \frac{g(t) - f_{\min}}{f_{\max} - f_{\min}}$$

Where $f(t)$, $g(t)$, $h(t)$ are the unprocessed, the detrended, and the preprocessed signals, respectively. t_0, t_1 are the time of the minimum value within the first and last 250 s of the signal, respectively, and m the slope of the detrending line. $f_{\min}$ and $f_{\max}$ are the minimum and maximum value of the detrended signal, respectively.

We focused most of our analyses on the GCaMP activity of individual CCAP neurons of the α class [25], whereas for the motoneurons we analyzed the total GCaMP activity on the left and right sides of the abdominal CNS, due to their large number. In preparations in which both CCAP and motoneurons expressed GCaMP, the 2 sets of neurons were readily distinguishable by their position and size.

Activity onset

The computation of activity onset was performed using a smoothened version of the time series, obtained by convolving the original time series with a rectangular window function of 10 s duration and area of 1. Onset was

defined as the first instant for which the convolved time series exceeded 1/2 of the maximum amplitude of the original time series. The first 100 s of the time series were discarded because some neurons displayed a high level of fluorescence at the beginning of the recordings.

Time frequency analyses

Time-frequency analyses were performed using the continuous wavelet transform (CWT) [55] with the complex Morlet wavelet (σ = 3). The CWT is defined by:

$$W(t,s) = \frac{1}{s}\int_{-\infty}^{\infty} f(u)\overline{\psi}\left(\frac{u-t}{s}\right)du$$

Where s is the scale parameter, t the position parameter, $f()$ the signal function, $\psi()$ the wavelet function and the overline represents the complex conjugate.

The complex Morlet is defined as:

$$\Psi_\sigma(t) = \left(1 + \exp(-\sigma^2) - 2\exp\left(-\frac{3}{4}\sigma^2\right)\right)^{-\frac{1}{2}} \pi^{-\frac{1}{4}} \exp\left(-\frac{1}{2}t^2\right)\left(\exp(i\sigma t) - \exp\left(-\frac{1}{2}\sigma^2\right)\right)$$

Which has a central frequency $\sim\sigma$ or central period $\sim 1/\sigma$.

The scaleogram, analog to the spectrogram, is defined as the square of the amplitude of the CWT:

$$X(t,s) = W(t,s)\overline{W(t,s)}$$

The scale is related to the period (T) in the following relationship:

$$T = \sim s/\sigma$$

Conductance based model

We adapted a CPG model developed by Jalil et al. (2010) by adding the $I_{i,CCAP}$ and $I_{i,X}$ terms, which represent currents generated by input from CCAP neurons and stochasticity, respectively; and by adding an equation that models the calcium fluorescence induced by neuronal activity.

$$\frac{dV_i}{dt}(t) = -\frac{I_{i,\mathrm{Na}} + I_{i,\mathrm{K}} + I_{i,\mathrm{L}} + I_{i,\mathrm{Syn}} + I_{i,\mathrm{CCAP}}(t) + I_{i,\mathrm{X}}}{C} \quad (1)$$

$$I_{i,\mathrm{Na}} = g_{\mathrm{Na}}(V_i - E_{\mathrm{Na}})n_i^3 h_i \quad (2)$$

$$I_{i,\mathrm{K}} = g_{\mathrm{K}}(V_i - E_{\mathrm{K}})m_i^2 \quad (3)$$

$$I_{i,\mathrm{L}} = g_{\mathrm{L}}(V_i - E_{\mathrm{L}}) \quad (4)$$

$$I_{i,\mathrm{Syn}} = g_{\mathrm{Syn}}(V_i - E_{\mathrm{Syn}})s\left(-1000\left(V_j + 0.0225\right)\right), \quad i \neq j \quad (5)$$

$$I_{i,\mathrm{CCAP}}(t) = g_{\mathrm{CCAP}}(V_i - E_{\mathrm{CCAP}})p(t) \quad (6)$$

$$dI_{i,\mathrm{X}} = -\frac{I_{i,\mathrm{X}}}{\tau_{\mathrm{X}}} + \sigma_{\mathrm{X}}W_{i,t} \quad (7)$$

$$n_i = s\left(-150(V_i + 0.0305)\right) \quad (8)$$

$$\frac{dh_i}{dt} = \frac{s\left(500(V_i + 0.0333)\right) - h_i}{\tau_{\mathrm{Na}}} \quad (9)$$

$$\frac{dm_i}{dt} = \frac{s\left(-83(V_i + V_{\mathrm{Shift}})\right) - m_i}{\tau_{\mathrm{K}}} \quad (10)$$

$$\frac{df_i}{dt} = \frac{s\left(-100(V_i + 0.04)\right) - f_i}{\tau_{\mathrm{f}}} \quad (11)$$

$$s(x) = \frac{1}{1 + exp(x)} \quad (12)$$

In this model, V is the membrane voltage, C, the membrane capacitance, and t, the time. I, g, E, τ , represent, respectively, the current, the maximum conductance, the reversal potential, and the time constant. The subscripts i, j refer to neuron index, Na, K, L, Syn, CCAP, X refer to sodium, potassium, leakage, synapse, CCAP, and noise (which is an Ornstein-Uhlenbeck process), respectively. $p(t)$ is the motoneuronal oscillation probability. W_t represents a Wiener process and σ_x its volatility. n, h, m are the sodium activating, sodium inactivating, and potassium activating gating variables, respectively; f represents the calcium imaging fluorescent intensity. V_{Shift} is a potassium activation curve shifting parameter.

Equation 6 was added to generate a depolarizing current during the predicted oscillatory phase. $p(t)$, the oscillating probability at time t from the logistic model, approaches 0 when the oscillation probability is low and 1

when it is high. In the conductance model, $p(t)$ acts as a gating variable, g_{CCAP} is the maximum conductance parameter and E_{CCAP} is the reversal potential. A high $p(t)$ value generates depolarizing currents that help the system reach the voltage threshold to fire action potentials (APs) in a bursting and alternating pattern between the neurons of the circuit. By contrast, a low $p(t)$ value tends to keep the system in a non-oscillatory state.

Equation 7 adds stochasticity to the model, which has the effect of mimicking the probabilistic influence of the α CCAP neurons on the motoneuronal oscillatory activity. It also adds phase noise during the oscillatory activity, similar to the one observed in the experimental recordings (Fig 4).

Equation 11 generates fluorescence (calcium) spikes, which respond with a time constant τ_f. The equation produces increases in the values of fluorescence during the bursting phase and decreases during the non-bursting phase.

Simulations were done using the following parameters: C=0.5 nF; τ_{Na}=0.055 s; g_{Na}=200 nS; g_K= 45 nS; g_L=10 nS; g_{Syn}=0.5 nS; g_{CCAP}=1 nS; E_{Na}=0.045 V; E_K=-0.07 V; E_L= -0.046 V; E_{Syn}=-0.0625 V; E_{CCAP}=0 V; V_{Shift}=0.022 V; τ_X=0.001 s; σ_X=0.03 nA.

The values for τ_K and τ_f varied as they were adjusted to each individual experiment. Their values are given in Table 2

Parameter	Experiment								
	1	2	3	4	5	6	7	8	9
τ_K (s)	55.2	63.9	125.6	67.7	136.5	71.5	71.5	69.0	88.1
τ_f (s)	3.2	4.1	11.2	10.0	11.2	4.8	8.6	3.7	4.4

Table 2. Values of τ_K and τ_f used for the fit of each experiments.

The oscillation period of the calcium spikes is affected by many parameters, but τ_K affects it linearly and does not affect the duty cycle and phase difference, making it much easier to adjust manually. The exponential decay on the other hand can only be fitted through τ_f and does not affect the model dynamics.

Time constants

The time constant for the fluorescence signal was computed by fitting an exponential decay function to the data, defined by:

$$f(t) = a \exp\left(\frac{-t}{\tau}\right) + b$$

Where a, b and τ are constants, a represents the amplitude of the decay, b the basal fluorescence, and τ the time constant. The time constant of a segment was defined to be the τ of the fitted 15 s template, which was adjusted through the least squares method.

The average time constant (τ_f) of the exponential decay of motoneuron calcium spikes was computed using only high quality (high SNR) segments of the recordings.

The time constant of the potassium gating variable (τK) was adjusted manually to make the periodicity of oscillations of the model match the previously measured periodicity of motoneuronal oscillation.

Puparium-free behavioral recordings and processing

Behavioral recordings were carried out as described in [25] Mena et al., 2016. Briefly, the pupa was surgically removed from the puparium at the very start of pre-ecdysis and placed in a recording chamber with halocarbon oil (Sigma-Aldrich Chemical Co., MO). The animals were filmed under transmitted light using a Leica DMLB microscope (20 X magnification) for at least 60 min.

Color RGB frames were extracted from the video sequence in real number format, with 0 and 1 representing the minimum and maximum intensity, respectively (Fig 9a). The images were converted to grayscale by averaging the intensity of the three-color component channels (Fig 9b). Pixels of the images were thresholded by setting them to 0 if the grayscale values were lower than 0.1 or to 1.0 otherwise (Fig 9c). Holes, or black regions inside white regions were then filled (Fig 9d). Although the value of the threshold was chosen arbitrarily, we found that the resulting thresholded image was not very sensitive to its exact value. To extract the main behavioral features, high spatial frequency details were removed in a two-step process. The images were first convolved with a gaussian function with $\sigma = 3$ pixels (Fig 9e) and then thresholded at a threshold of 0.5, to avoid expanding (dilating) or reducing (eroding) the borders of the pupa (Fig 9f). Regions with less than 10000 white pixels, roughly

624 20% of the area of the pupa (see Fig 9g) were discarded. The left- and rightmost pixels of the pupa along the
625 anteroposterior axis were then computed. The average between the left- and rightmost pixels along the axis were
626 considered to represent the midline of the pupa (Fig 9h).

627

628 # REFERENCES

629

630 1. Lisman JE, Idiart MA. Storage of 7 +/- 2 short-term memories in oscillatory subcycles. Science. 1995;267:
631 1512–5. doi:10.1126/science.7878473

632 2. Clapp WC, Rubens MT, Sabharwal J, Gazzaley A. Deficit in switching between functional brain networks
633 underlies the impact of multitasking on working memory in older adults. Proc Natl Acad Sci. 2011;108:
634 7212–7217. doi:10.1073/pnas.1015297108

635 3. Gray CM. Synchronous oscillations in neuronal systems: mechanisms and functions. J Comput Neurosci.
636 1994;1: 11–38. doi:10.1007/BF00962716

637 4. Laurent G, Davidowitz H. Encoding of olfactory information with oscillating neural assemblies. Science.
638 1994;265: 1872–5. doi:10.1126/science.265.5180.1872

639 5. Laurent G, Naraghi M. Odorant-induced oscillations in the mushroom bodies of the locust. J Neurosci.
640 1994;14: 2993–3004. Available: http://www.ncbi.nlm.nih.gov/pubmed/8182454

641 6. Wehr M, Laurent G. Odour encoding by temporal sequences of firing in oscillating neural assemblies.
642 Nature. 1996;384: 162–6. doi:10.1038/384162a0

643 7. Ramirez J-M, Tryba AK, Peña F. Pacemaker neurons and neuronal networks: an integrative view. Curr
644 Opin Neurobiol. 2004;14: 665–74. doi:10.1016/j.conb.2004.10.011

645 8. Grillner S. Biological pattern generation: the cellular and computational logic of networks in motion.
646 Neuron. 2006;52: 751–66. doi:10.1016/j.neuron.2006.11.008

9. Dickinson PS. Neuromodulation of central pattern generators in invertebrates and vertebrates. Curr Opin Neurobiol. 2006;16: 604–614. doi:10.1016/j.conb.2006.10.007

10. Garcia-Campmany L, Stam FJ, Goulding M. From circuits to behaviour: motor networks in vertebrates. Curr Opin Neurobiol. 2010;20: 116–125. doi:10.1016/j.conb.2010.01.002

11. Dubowy CM, Cavanaugh DJ. Sleep: a neuropeptidergic wake-up call for flies. Curr Biol. 2014;24: R1092-4. doi:10.1016/j.cub.2014.10.020

12. Bargmann CI, Marder E. From the connectome to brain function. Nat Methods. 2013;10: 483–90. doi:10.1038/nmeth.2451

13. Selverston AI. Invertebrate central pattern generator circuits. Philos Trans R Soc Lond B Biol Sci. 2010;365: 2329–45. doi:10.1098/rstb.2009.0270

14. Zhao Y, Bretz CA, Hawksworth SA, Hirsh J, Johnson EC. Corazonin neurons function in sexually dimorphic circuitry that shape behavioral responses to stress in Drosophila. PLoS One. 2010;5: e9141. doi:10.1371/journal.pone.0009141

15. Yapici N, Kim Y-J, Ribeiro C, Dickson BJ. A receptor that mediates the post-mating switch in Drosophila reproductive behaviour. Nature. 2008;451: 33–7. doi:10.1038/nature06483

16. Feany MB, Quinn WG. A neuropeptide gene defined by the Drosophila memory mutant amnesiac. Science. 1995;268: 869–73. doi:10.1126/science.7754370

17. Reynolds SE. Integration of Behaviour and Physiology in Ecdysis. Adv In Insect Phys. 1980;15: 475–595. doi:10.1016/S0065-2806(08)60144-7

18. Ewer J, Reynolds S. Neuropeptide Control of Molting in Insects. Hormones, Brain and Behavior. Academic Press; 2002. pp. 1–XVI. doi:10.1016/B978-012532104-4/50037-8

19. Mesce KA, Fahrbach SE. Integration of endocrine signals that regulate insect ecdysis. Front Neuroendocrinol. 2002;23: 179–99. doi:10.1006/frne.2002.0228

20. Zitnan D, Adams ME. 3.1 - Neuroendocrine Regulation of Insect Ecdysis. In: Gilbert LIBT-CMIS, editor.

671 Comprehensive Molecular Insect Science. Amsterdam: Elsevier; 2005. pp. 1–60.
672 doi:https://doi.org/10.1016/B0-44-451924-6/00032-6

673 21. Gammie SC, Truman JW. Neuropeptide hierarchies and the activation of sequential motor behaviors in the
674 hawkmoth, Manduca sexta. J Neurosci. 1997;17: 4389–4397. Available:
675 papers3://publication/uuid/B3A812E0-B612-47EF-B786-292174EE5657

676 22. Kim Y-J, Zitnan D, Galizia CG, Cho K-H, Adams ME. A command chemical triggers an innate behavior by
677 sequential activation of multiple peptidergic ensembles. Curr Biol. 2006;16: 1395–1407.
678 doi:10.1016/j.cub.2006.06.027

679 23. Lahr EC, Dean D, Ewer J. Genetic analysis of ecdysis behavior in Drosophila reveals partially overlapping
680 functions of two unrelated neuropeptides. J Neurosci. 2012;32: 6819–6829.
681 doi:10.1523/JNEUROSCI.5301-11.2012

682 24. Kim D-H, Han M-R, Lee G, Lee SS, Kim Y-J, Adams ME. Rescheduling Behavioral Subunits of a Fixed
683 Action Pattern by Genetic Manipulation of Peptidergic Signaling. Schoofs L, editor. PLOS Genet. 2015;11.
684 doi:10.1371/journal.pgen.1005513

685 25. Mena W, Diegelmann S, Wegener C, Ewer J. Stereotyped responses of Drosophila peptidergic neuronal
686 ensemble depend on downstream neuromodulators. Elife. 2016;5: 22. doi:10.7554/eLife.19686

687 26. Diao F, Mena W, Shi J, Park D, Diao F, Taghert P, et al. The splice isoforms of the Drosophila ecdysis
688 triggering hormone receptor have developmentally distinct roles. Genetics. 2016;202: 175–189.
689 doi:10.1534/genetics.115.182121

690 27. Diao F, Elliott AD, Diao F, Shah S, White BH. Neuromodulatory connectivity defines the structure of a
691 behavioral neural network. Elife. 2017;6: 1–30. doi:10.7554/eLife.29797

692 28. Lemon WC, Pulver SR, Höckendorf B, McDole K, Branson K, Freeman J, et al. Whole-central nervous
693 system functional imaging in larval Drosophila. Nat Commun. 2015;6: 7924. doi:10.1038/ncomms8924

694 29. Kato S, Kaplan HS, Schrödel T, Skora S, Lindsay TH, Yemini E, et al. Global brain dynamics embed the
695 motor command sequence of Caenorhabditis elegans. Cell. 2015;163: 656–69.

doi:10.1016/j.cell.2015.09.034

30. Freeman J, Vladimirov N, Kawashima T, Mu Y, Sofroniew NJ, Bennett D V, et al. Mapping brain activity at scale with cluster computing. Nat Methods. 2014;11: 941–50. doi:10.1038/nmeth.3041

31. Loveall BJ, Deitcher DL. The essential role of bursicon during drosophila development. BMC Dev Biol. 2010;10. doi:10.1186/1471-213X-10-92

32. Karsai G, Pollák E, Wacker M, Vömel M, Selcho M, Berta G, et al. Diverse in- and output polarities and high complexity of local synaptic and non-synaptic signaling within a chemically defined class of peptidergic Drosophila neurons. Front Neural Circuits. 2013;7: 1–22. doi:10.3389/fncir.2013.00127

33. Hughes CL, Thomas JB. A sensory feedback circuit coordinates muscle activity in Drosophila. Mol Cell Neurosci. 2007;35: 383–396. doi:10.1016/j.mcn.2007.04.001

34. Sporns O. Terzahi_1956_Conference_Submarine Landslides.pdf. 2013; 247–262.

35. Akaike H. A new look at the statistical model identification. IEEE Trans Automat Contr. 1974;19: 716–723. doi:10.1109/TAC.1974.1100705

36. Jalil S, Belykh I, Shilnikov A. Fast reciprocal inhibition can synchronize bursting neurons. Phys Rev E - Stat Nonlinear, Soft Matter Phys. 2010;81: 1–4. doi:10.1103/PhysRevE.81.045201

37. Nässel DR. Neuropeptide signaling near and far: how localized and timed is the action of neuropeptides in brain circuits? Invert Neurosci. 2009;9: 57–75. doi:10.1007/s10158-009-0090-1

38. Ludwig M, Leng G. Dendritic peptide release and peptide-dependent behaviours. Nat Rev Neurosci. 2006;7: 126–136. doi:10.1038/nrn1845

39. Nusbaum MP, Blitz DM, Marder E. Functional consequences of neuropeptide and small-molecule co-transmission. Nat Rev Neurosci. 2017;18: 389–403. doi:10.1038/nrn.2017.56

40. Nässel DR. Substrates for Neuronal Cotransmission With Neuropeptides and Small Molecule Neurotransmitters in Drosophila. Front Cell Neurosci. 2018;12. doi:10.3389/fncel.2018.00083

41. Szabo V, Ventalon C, De Sars V, Bradley J, Emiliani V. Spatially selective holographic photoactivation and

functional fluorescence imaging in freely behaving mice with a fiberscope. Neuron. 2014;84: 1157–69. doi:10.1016/j.neuron.2014.11.005

42. Hernandez O, Papagiakoumou E, Tanese D, Fidelin K, Wyart C, Emiliani V. Three-dimensional spatiotemporal focusing of holographic patterns. Nat Commun. 2016;7. doi:10.1038/ncomms11928

43. Shemesh OA, Tanese D, Zampini V, Linghu C, Piatkevich K, Ronzitti E, et al. Temporally precise single-cell-resolution optogenetics. Nat Neurosci. 2017;20: 1796–1806. doi:10.1038/s41593-017-0018-8

44. Shilnikov A, Cymbalyuk G. Transition between tonic spiking and bursting in a neuron model via the blue-sky catastrophe. Phys Rev Lett. 2005;94: 48101. doi:10.1103/PhysRevLett.94.048101

45. Marder E, Taylor AL. Multiple models to capture the variability in biological neurons and networks. Nat Neurosci. 2011;14: 133–138. doi:10.1038/nn.2735

46. Marder E. Variability, compensation, and modulation in neurons and circuits. Proc Natl Acad Sci U S A. 2011;108 Suppl: 15542–15548. doi:10.1073/pnas.1010674108

47. Gjorgjieva J, Drion G, Marder E. Computational implications of biophysical diversity and multiple timescales in neurons and synapses for circuit performance. Curr Opin Neurobiol. 2016;37: 44–52. doi:10.1016/j.conb.2015.12.008

48. Büschges A, Akay T, Gabriel JP, Schmidt J. Organizing network action for locomotion: Insights from studying insect walking. Brain Res Rev. 2008;57: 162–171. doi:10.1016/j.brainresrev.2007.06.028

49. Ayali A, Couzin-Fuchs E, David I, Gal O, Holmes P, Knebel D. Sensory feedback in cockroach locomotion: current knowledge and open questions. J Comp Physiol A Neuroethol Sensory, Neural, Behav Physiol. 2015;201: 841–850. doi:10.1007/s00359-014-0968-1

50. Gjorgjieva J, Berni J, Evers JF, Eglen SJ. Neural circuits for peristaltic wave propagation in crawling Drosophila larvae: analysis and modeling. Front Comput Neurosci. 2013;7: 1–19. doi:10.3389/fncom.2013.00024

51. Fushiki A, Zwart MF, Kohsaka H, Fetter RD, Cardona A, Nose A. A circuit mechanism for the propagation of waves of muscle contraction in Drosophila. Elife. 2016;5: 1–23. doi:10.7554/eLife.13253

745 52. Park JH, Schroeder AJ, Helfrich-Förster C, Jackson FR, Ewer J. Targeted ablation of CCAP neuropeptide-
746 containing neurons of Drosophila causes specific defects in execution and circadian timing of ecdysis
747 behavior. Development. 2003;130: 2645–2656. doi:10.1242/dev.00503

748 53. Torroja L, Packard M, Gorczyca M, White K, Budnik V. The Drosophila beta-amyloid precursor protein
749 homolog promotes synapse differentiation at the neuromuscular junction. J Neurosci. 1999;19: 7793–
750 7803. Available: http://www.ncbi.nlm.nih.gov/pubmed/10479682

751 54. Schneider CA, Rasband WS, Eliceiri KW. NIH Image to ImageJ: 25 years of image analysis. Nat Methods.
752 2012;9: 671–675. doi:10.1038/nmeth.2089

753 55. Bertrand O, Tallon-Baudry C, Pernier J. Time-Frequency Analysis of Oscillatory Gamma-Band Activity:
754 Wavelet Approach and Phase-Locking Estimation. Biomag 96. New York, NY: Springer New York; 2000.
755 pp. 919–922. doi:10.1007/978-1-4612-1260-7_224

756

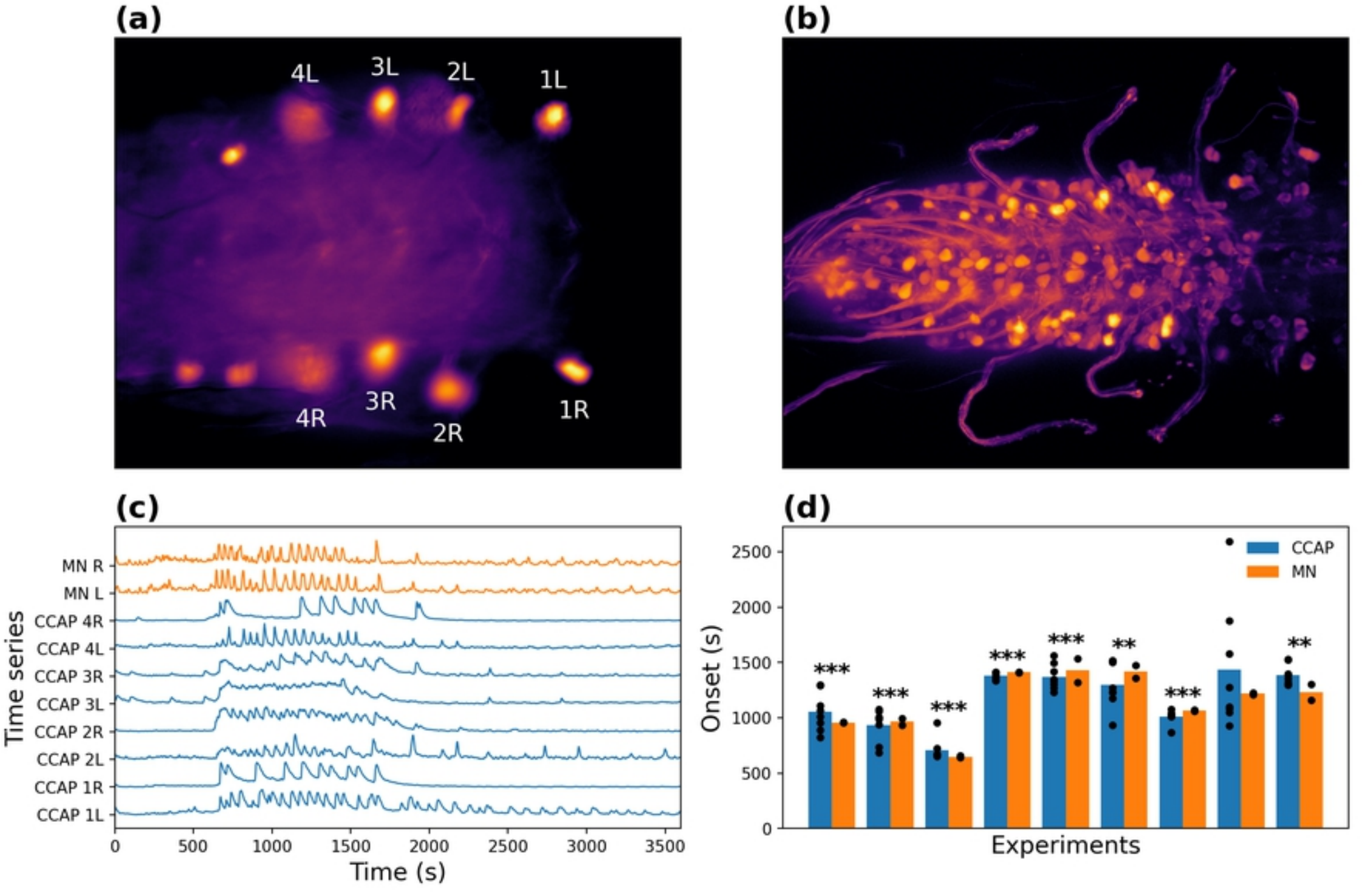
(a)
4L
3L
2L
1L
4R
3R
2R
1R
(b)
(c)
MN R
MN L
CCAP 4R
CCAP 4L
CCAP 3R
CCAP 3L
CCAP 2R
CCAP 2L
CCAP 1R
CCAP 1L
Time series
0
500
1000
1500
2000
2500
3000
3500
Time (s)
(d)
CCAP
MN
Onset (s)
0
500
1000
1500
2000
2500
***
***
***
***
***
**
***
**
Experiments

Figure 1

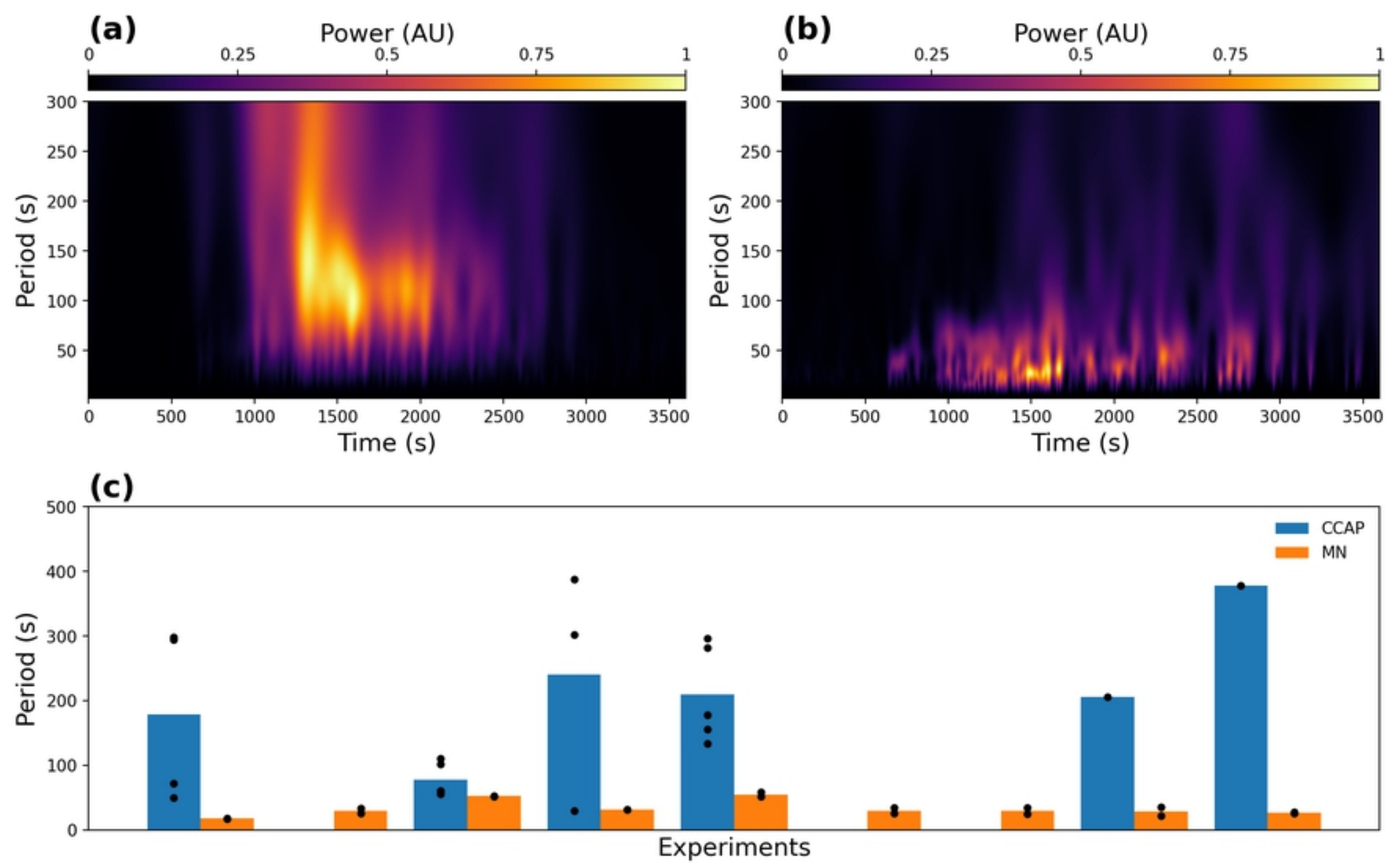
(a)
Power (AU)
0
0.25
0.5
0.75
1
Period (s)
300
250
200
150
100
50
0
500
1000
1500
2000
2500
3000
3500
Time (s)
(b)
Power (AU)
0
0.25
0.5
0.75
1
Period (s)
300
250
200
150
100
50
0
500
1000
1500
2000
2500
3000
3500
Time (s)
(c)
Period (s)
500
400
300
200
100
0
CCAP
MN
Experiments

Figure 2

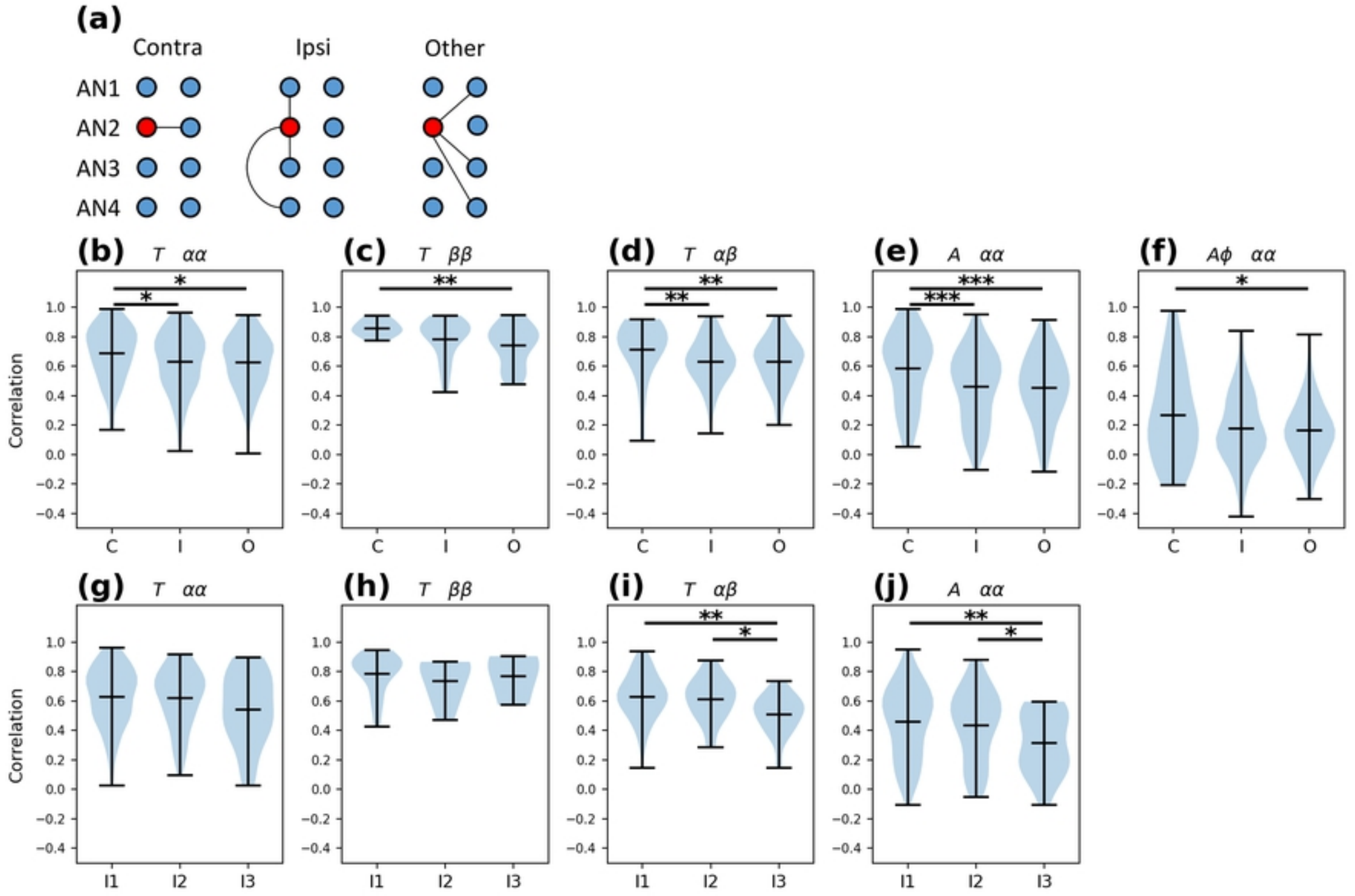
(a)
Contra
Ipsi
Other
AN1
AN2
AN3
AN4
(b) T αα
(c) T ββ
(d) T αβ
(e) A αα
(f) Aϕ αα
(g) T αα
(h) T ββ
(i) T αβ
(j) A αα
Correlation
C
I
O
I1
I2
I3

Figure 3

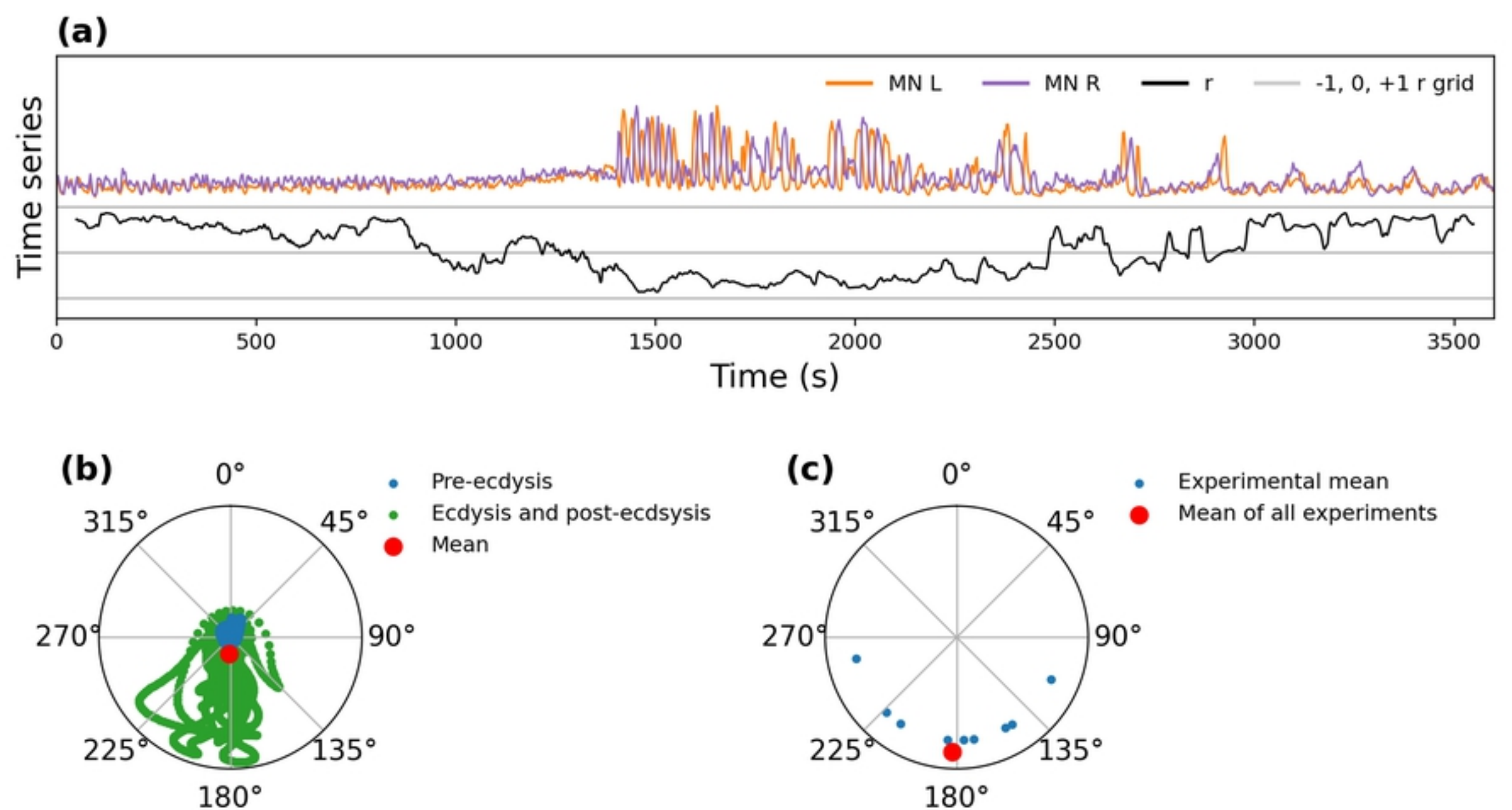
(a)
MN L
MN R
r
-1, 0, +1 r grid
Time series
0
500
1000
1500
2000
2500
3000
3500
Time (s)
(b)
0°
45°
90°
135°
180°
225°
270°
315°
Pre-ecdysis
Ecdysis and post-ecdsysis
Mean
(c)
0°
45°
90°
135°
180°
225°
270°
315°
Experimental mean
Mean of all experiments

Figure 4

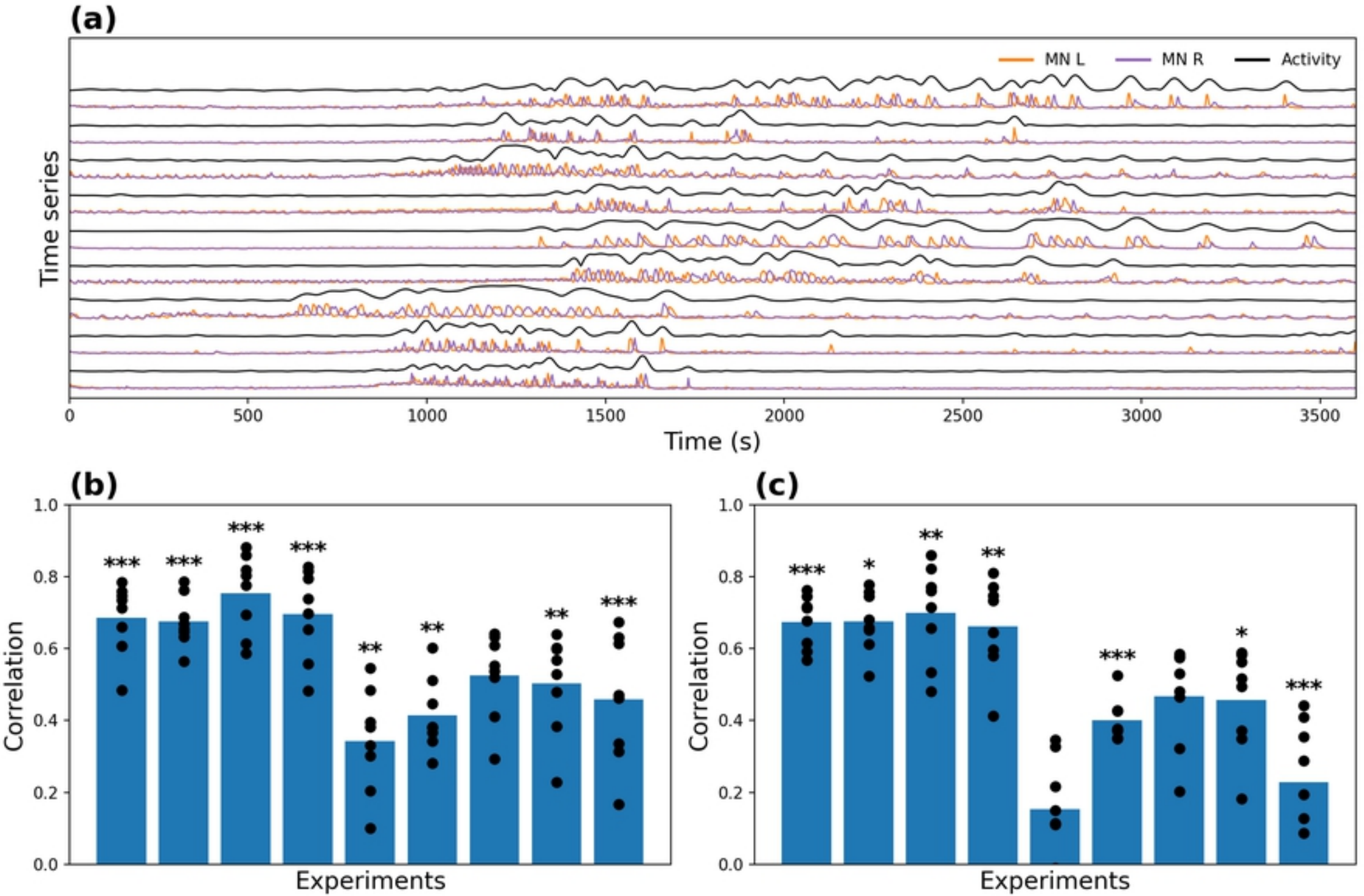
(a)
MN L
MN R
Activity
Time series
0
500
1000
1500
2000
2500
3000
3500
Time (s)
(b)
Correlation
1.0
0.8
0.6
0.4
0.2
0.0
***
***
***
***
**
**
**
**
***
Experiments
(c)
Correlation
1.0
0.8
0.6
0.4
0.2
0.0
***
*
**
**
***
*
***
Experiments

Figure 5

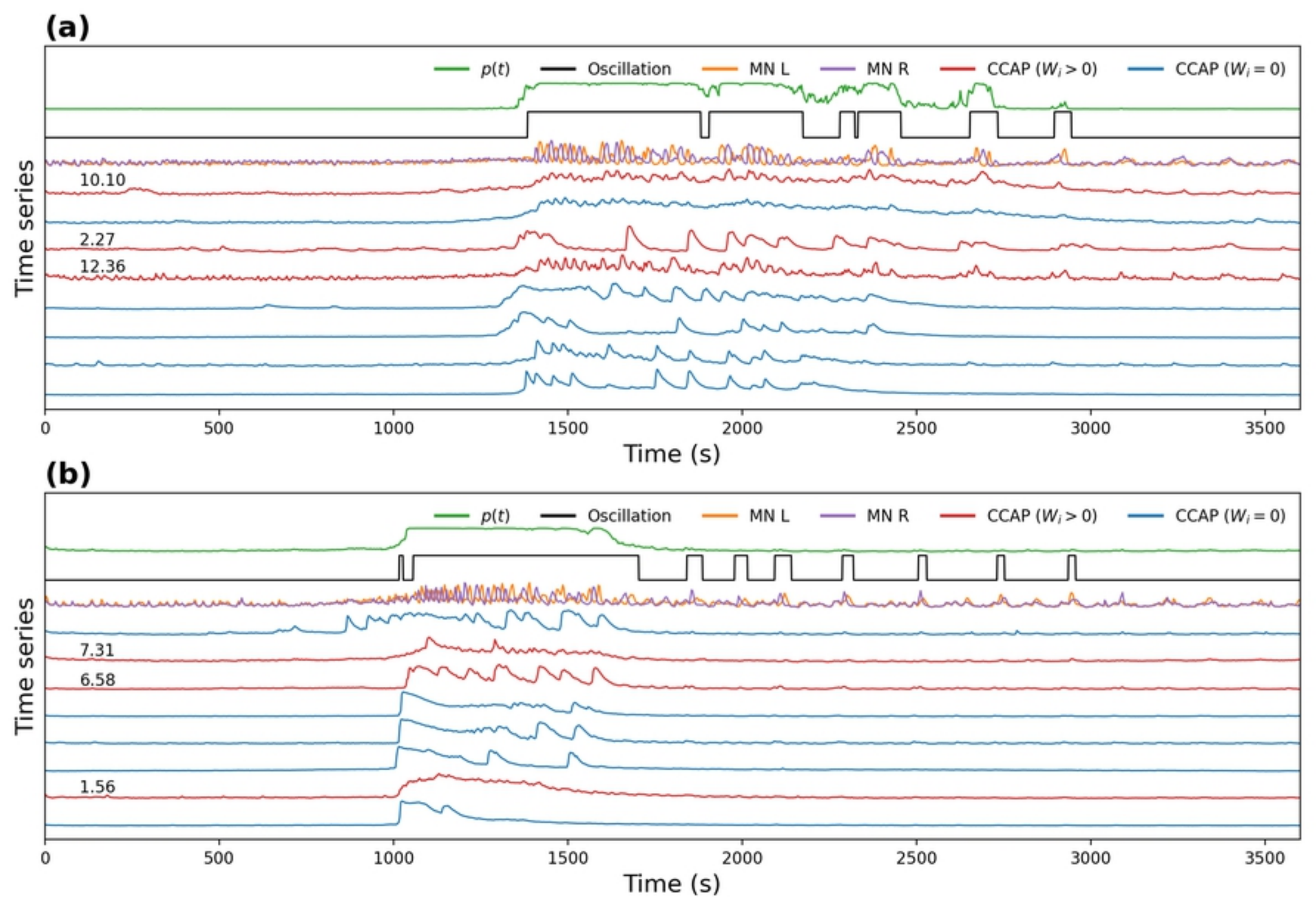
(a)
p(t)
Oscillation
MN L
MN R
CCAP ($W_i > 0$)
CCAP ($W_i = 0$)
Time series
10.10
2.27
12.36
0
500
1000
1500
2000
2500
3000
3500
Time (s)
(b)
p(t)
Oscillation
MN L
MN R
CCAP ($W_i > 0$)
CCAP ($W_i = 0$)
Time series
7.31
6.58
1.56
0
500
1000
1500
2000
2500
3000
3500
Time (s)

Figure 6

Figure 7

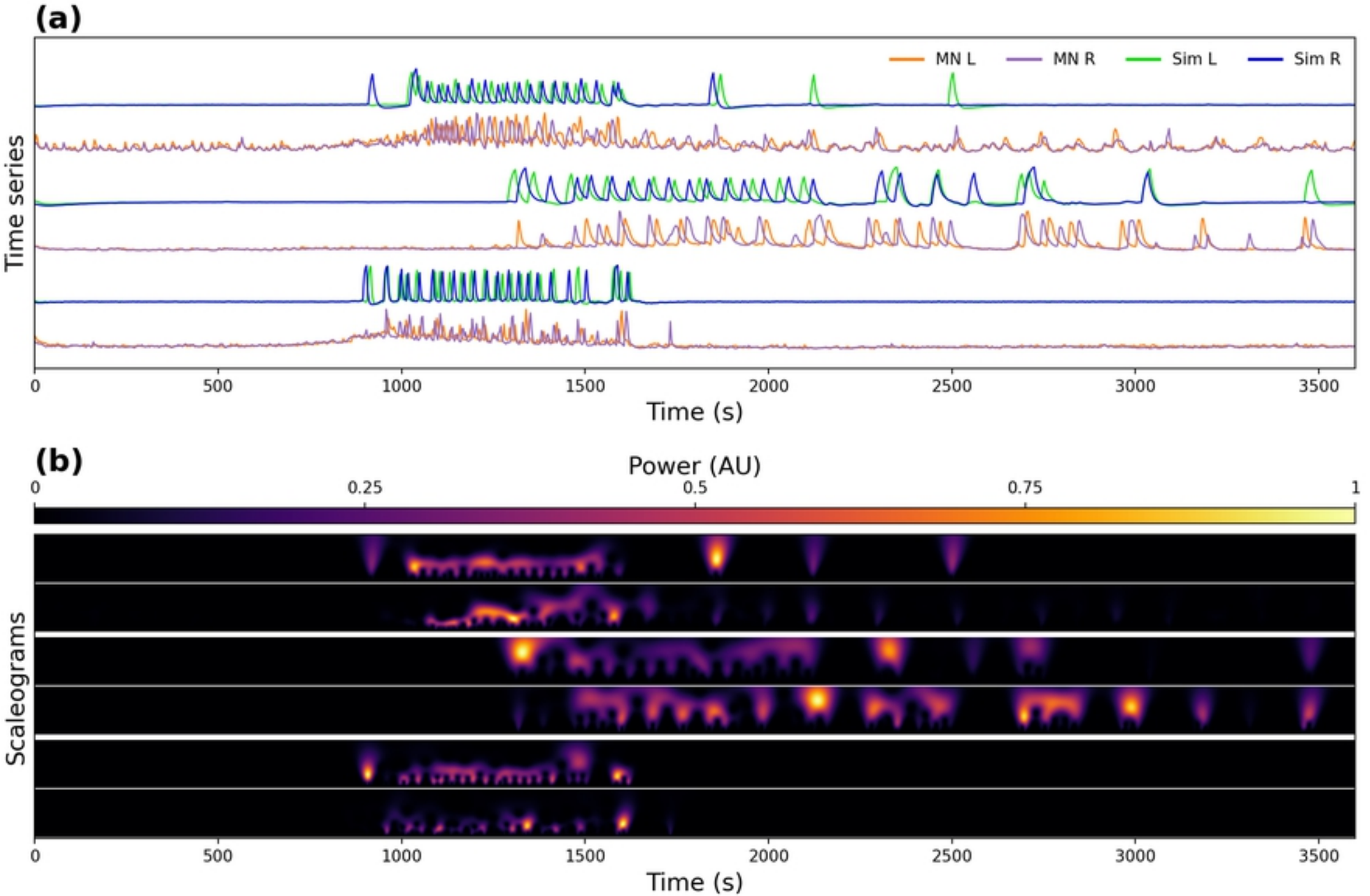
(a)
MN L
MN R
Sim L
Sim R
Time series
0
500
1000
1500
2000
2500
3000
3500
Time (s)
(b)
Power (AU)
0
0.25
0.5
0.75
1
Scaleograms
0
500
1000
1500
2000
2500
3000
3500
Time (s)

Figure 8

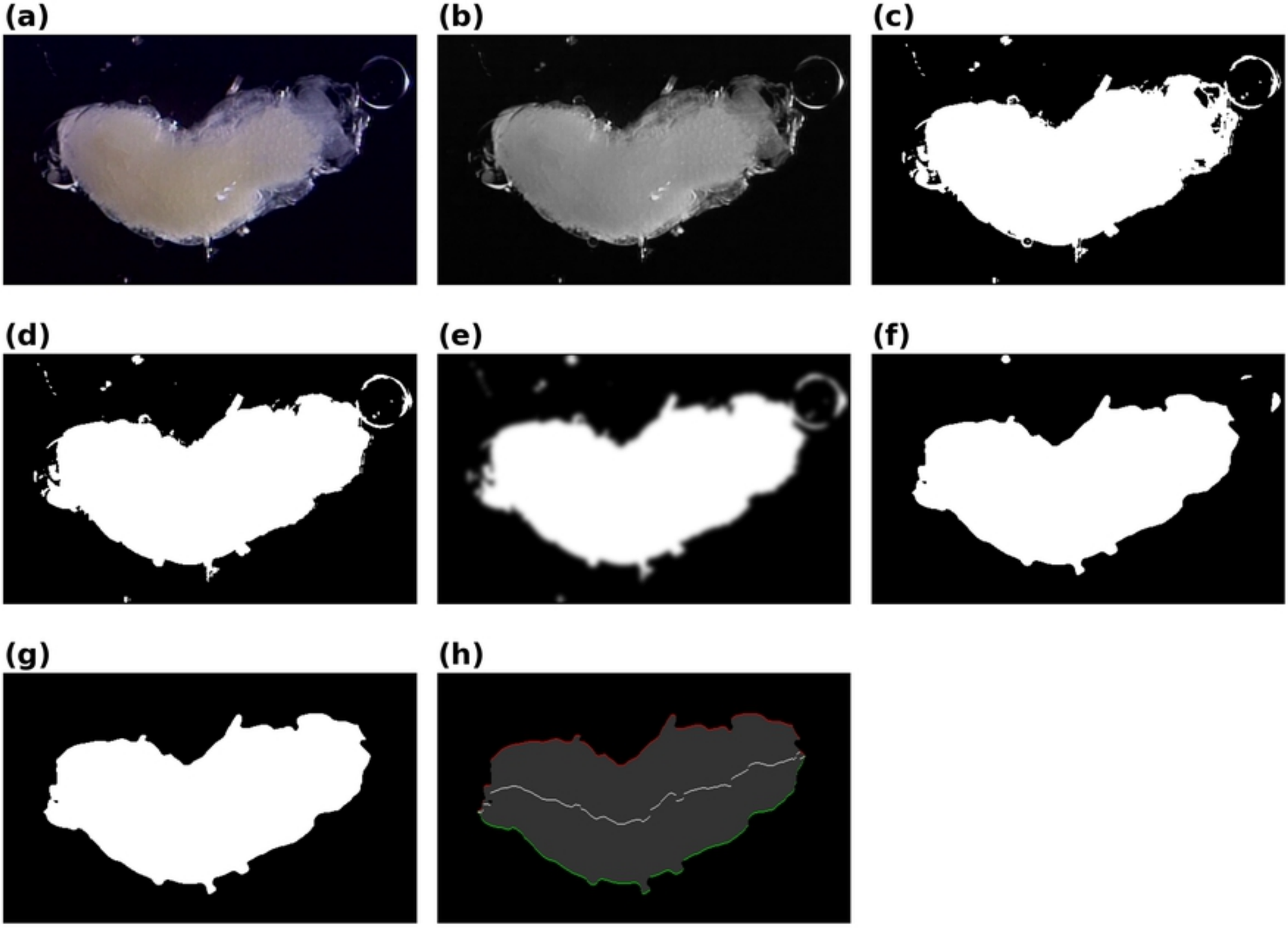

Figure 9

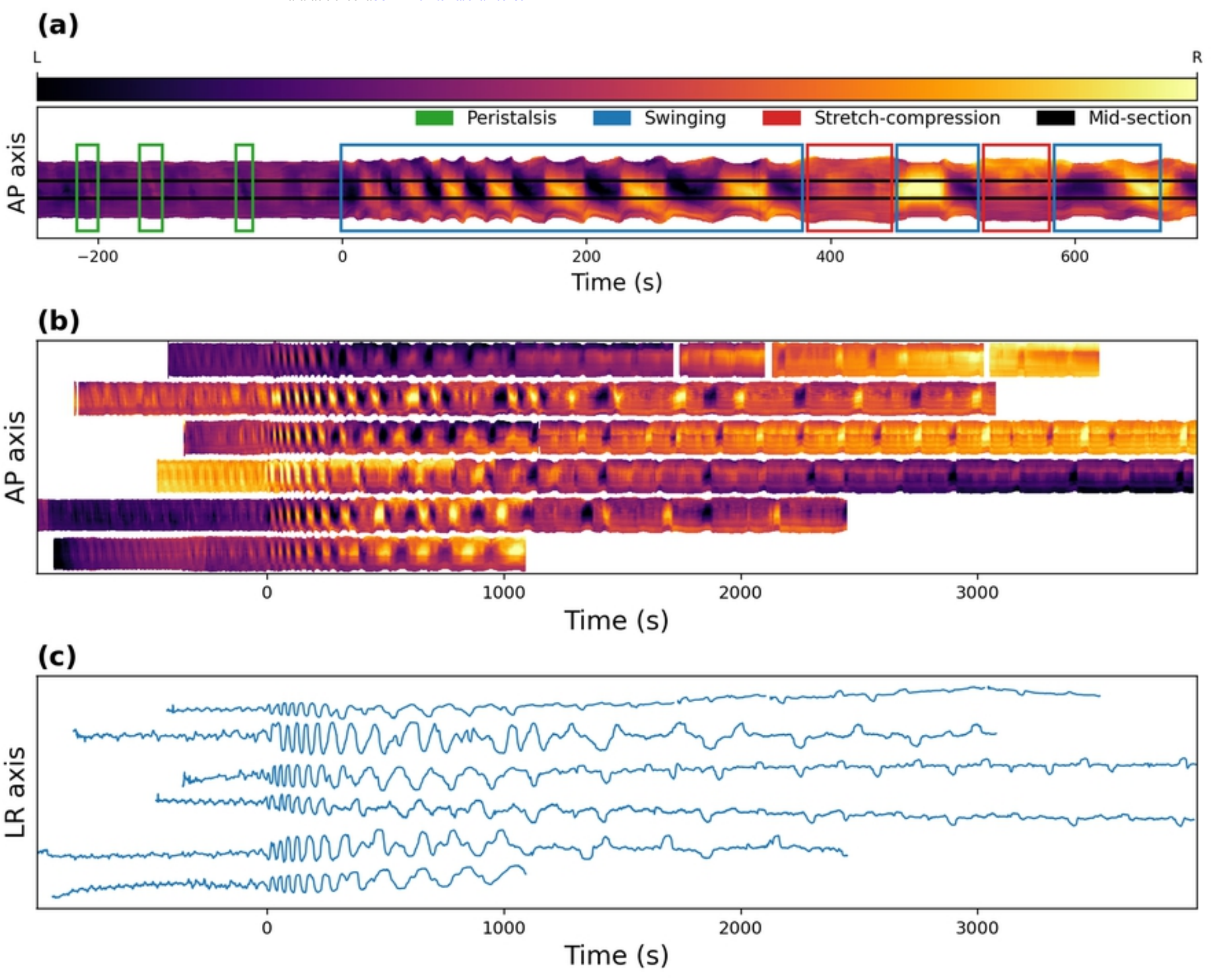
(a)
L
R
Peristalsis
Swinging
Stretch-compression
Mid-section
AP axis
−200
0
200
400
600
Time (s)
(b)
AP axis
0
1000
2000
3000
Time (s)
(c)
LR axis
0
1000
2000
3000
Time (s)

Figure 10

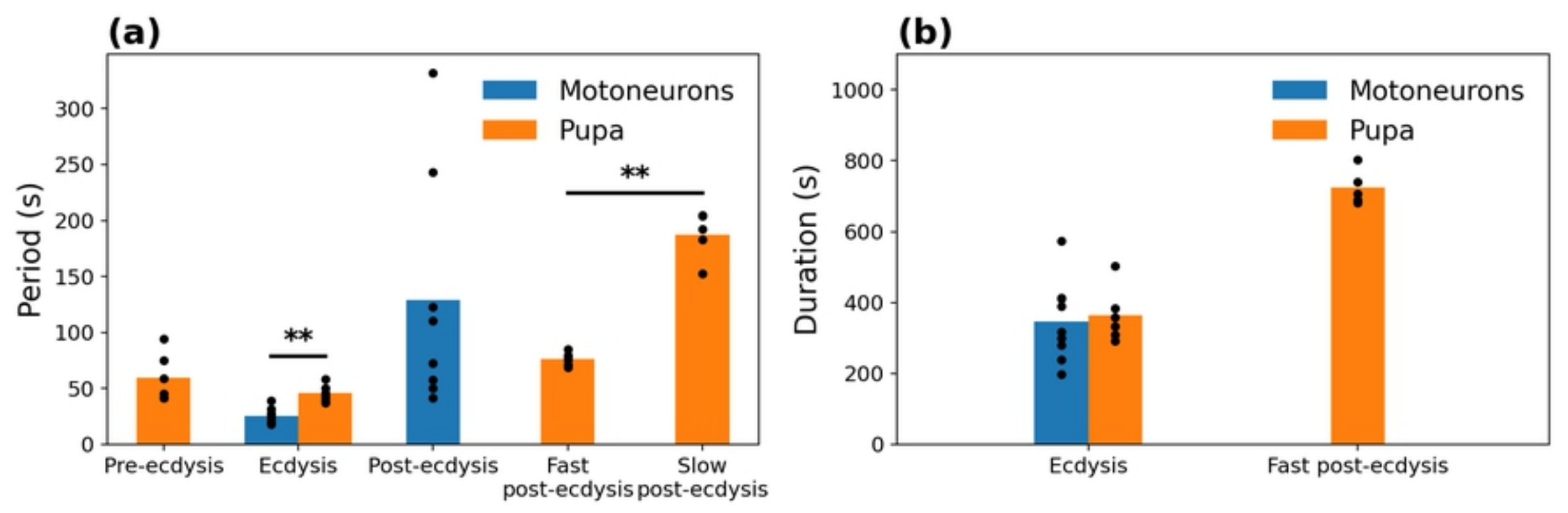
(a)
Period (s)
0
50
100
150
200
250
300
Motoneurons
Pupa
**
**
Pre-ecdysis
Ecdysis
Post-ecdysis
Fast post-ecdysis
Slow post-ecdysis
(b)
Duration (s)
0
200
400
600
800
1000
Motoneurons
Pupa
Ecdysis
Fast post-ecdysis

Figure 11